Moiré Superstructures of Graphene on Faceted Nickel Islands

Yuya Murata,[†] Vania Petrova,[§] Branden B. Kappes,[‡] Abbas Ebnonnasir,[‡] Ivan Petrov,[§] Ya-Hong Xie,[†] Cristian V. Ciobanu,[‡] and Suneel Kodambaka[†,*]

[†]Department of Materials Science and Engineering, University of California Los Angeles, Los Angeles, California 90095, United States, [§]Frederick Seitz Materials Research Laboratory, University of Illinois, Urbana, Illinois 61801, United States, and [‡]Division of Engineering, Colorado School of Mines, Golden, Colorado 80401, United States

ABSTRACT Using scanning tunneling microscopy and spectroscopy, in combination with density functional theory calculations, we investigated the morphology and electronic structure of monolayer graphene grown on the (111) and (110) facets of three-dimensional nickel islands on highly oriented pyrolytic graphite substrate. We observed graphene domains exhibiting hexagonal and striped moiré patterns with periodicities of 22 and 12 Å, respectively, on (111) and (110) facets of the Ni islands. Graphene domains are also observed to grow, as single crystals, across adjacent facets and over facet boundaries. Scanning tunneling spectroscopy data indicate that the graphene layers are metallic on both Ni(111) and Ni(110), in agreement with the calculations. We attribute this behavior to a strong hybridization between the d-bands on Ni and the π-bands of carbon. Our findings point to the possibility of preparing large-area epitaxial graphene layers even on polycrystalline Ni substrates.

KEYWORDS: graphene · nickel · three-dimensional island · scanning tunneling microscopy/spectroscopy · density functional theory · electronic structure

Graphene, a two-dimensional (2D) single crystal of carbon atoms arranged in a honeycomb lattice,[1] is attractive for applications in nanoelectromechanical devices,[2] in high-performance low-power electronics,[3] and as transparent electrodes.[4] To date, epitaxial graphene layers have been synthesized *via* thermal carburization of SiC(0001)[5] and by surface segregation of carbon dissolved in the bulk or by chemical vapor deposition (CVD) of carbon on single-crystalline metal (Ni, Cu, Ir, Ru, and Pt),[6−11] and insulating (h-BN) surfaces.[12] Recent studies indicate that large-area graphene layers of controllable thicknesses can also be synthesized *via* CVD on polycrystalline Ni and Cu foils or thin films.[4,13] In these experiments, graphene layer morphology is found to depend on cooling rates and is also likely to vary with the substrate or film crystallinity.[14,15] However, relatively little is known concerning the role of substrate microstructure (grain size, shape, and orientation) on the nucleation and growth of graphene. Here, we focus on understanding the influence of metal surface orientation on the morphology and structure of graphene.

To this purpose, we choose Ni as the model material. We prepared isolated 3D Ni islands, composed of crystalline facets of different orientations, to serve as a polycrystalline surface. Highly oriented pyrolytic graphite (HOPG) is chosen as a substrate for Ni deposition because it is relatively inert, less likely to introduce any strain into the Ni islands, and also serves as a source of carbon for the growth of graphene. Using ultrahigh vacuum scanning tunneling microscopy (UHV-STM), we investigated the growth and structure of graphene on the Ni islands. We observed monolayer graphene domains on (111) and (110) surfaces of Ni islands upon annealing the samples in UHV at 700 °C for 2 h. STM images of graphene on Ni(111) show hexagonal close-packed moiré patterns with a periodicity of 22 Å. On Ni(110), we observe stripe patterns with a periodicity of 12 Å. Surprisingly, graphene domains are also observed to grow seamlessly, as single crystals, across adjacent (111) and (110) facets and over the facet boundary. Scanning tunneling spectroscopy (STS) measurements indicate that graphene layers are metallic on both (111) and (110) surfaces of Ni. Density functional theory (DFT) calculations of the partial density of states also show that the graphene layers are metallic; this is consistent with the STS data and is due to a strong hybridization of the d-bands of Ni and the π-bands of carbon.

*Address correspondence to kodambaka@ucla.edu.

Received for review July 2, 2010 and accepted October 07, 2010.

Published online October 14, 2010.
10.1021/nn102446y

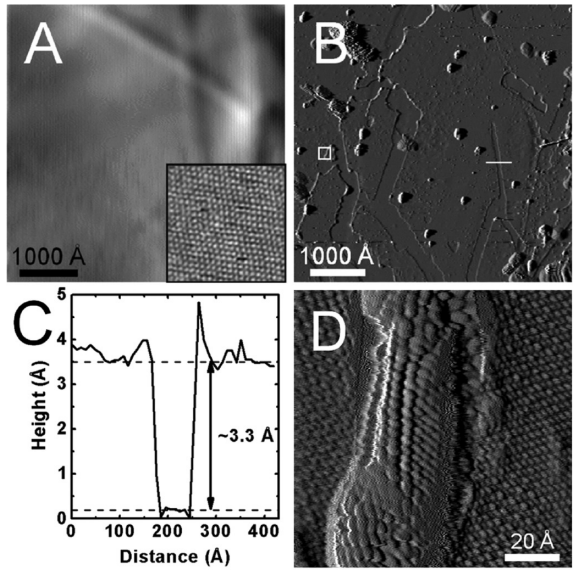

Figure 1. Differentiated room-temperature STM images of (A) clean HOPG surface (4750 × 4750 Å²) and (B) Ni-covered HOPG surface (5000 × 5000 Å²) after annealing at 700 °C for 2 h. The inset in panel A is an atomic-resolution STM image (50 × 50 Å²) of HOPG surface. (C) Line profile along the white line across a trench in B. (D) Higher-resolution STM image (100 × 100 Å²) of the white rectangular region in B.

RESULTS AND DISCUSSION

Graphene Formation on 3D Ni Islands. Figure 1A is a typical room-temperature STM image acquired from a clean HOPG surface showing atomically flat terraces. The characteristic triangular lattice of graphite is visible in the atomic-resolution image (see inset). In order to obtain isolated 3D Ni islands, ~3 Å thick Ni is evaporated onto the surface at room temperature and annealed in UHV at 400 °C for times between 1 and 2 h. As a result, we obtain 3D faceted Ni islands on the substrate; that is, Ni atoms did not intercalate under the graphite surface.[16−18] From the STM images of the islands, we determine the top surface facet orientations to be either {111} or {110}, consistent with previous reports.[19] The average height and width of the Ni islands are ~100 and ~1000 Å, respectively.

Annealing the samples at temperatures above 650 °C in UHV leads to the formation of graphene on top of the Ni islands. Figure 1B is a representative room-temperature STM image acquired from the sample after annealing at 700 °C for 2 h. The image shows 3D Ni islands along with ~100 Å wide trenches, bounded by single-atom-height steps (Figure 1C). From the atomic-resolution STM image (Figure 1D), we find that the trenches are composed of graphite with steps oriented along $\langle 11\bar{2}0 \rangle$. These trenches are presumably a direct consequence of substrate etching *via* carbon dissolution in the metal.[20−24] (We rule out evaporation of both C and Ni from the surface at these temperatures.) The dissolved carbon can precipitate as graphene on the surface of Ni islands upon cooling.[25] We show in the following sections that a similar process leads to graphene formation on {111} and {110} facets of the Ni islands.

Graphene on Ni(111). Figure 2A is a typical STM image of a 3D Ni island acquired after annealing the sample at 700 °C for 2 h. The top surface shows a hexagonal array of circular features, while the side facet exhibits a stripe pattern. Figure 2B is an atomic-resolution image of the region highlighted by a rectangle in Figure 2A. The image shows a hexagonal lattice with a periodicity of ~2.5 Å, which is assigned to single-layer graphene. (In case of multilayer graphene, triangular lattice as in Figure 1A is expected.) Note the variation in atomic arrangement across the white dashed line in Figure 2B, although there is no difference in the surface height. That is, the graphene layer on the top surface is composed of two rotational domains,[9,26,27] which are color-coded for clarity in Figure 2C. Here, the presence of two domains on the same surface suggests simultaneous nucleation and growth of graphene at two different sites on the island.

We now focus on the structure of the graphene layers formed on the Ni islands. The ordered structure on the top surface of the island in Figure 2A is a moiré pattern formed by the superposition of graphene and Ni lattices. (Similar patterns have also been observed on other metal surfaces.[27]) From the STM image in Figure 2B, we measure a spatial periodicity of ~22 Å for the hexagonal pattern. This is typical of most graphene islands observed in our experiments; however, we have also observed moiré patterns with periodicities as small as 15 Å, but they are relatively few.

In order to explain the observed hexagonal moiré pattern in the larger graphene domain (colored green in Figure 2C), we assumed that the Ni island surface orientation is Ni(111) (justified later) and constructed an atomic model of graphene/Ni superstructure using the in-plane lattice constants of graphene (2.46 Å) and Ni(111) (2.49 Å). The moiré pattern with 22 Å periodicity is obtained when graphene $[11\bar{2}0]$ is rotated by an angle θ = 6.4° with respect to Ni[110]. The geometry of such an incommensurate moiré superstructure, along with the determined epitaxial relationship between graphene and Ni(111), is shown in Figure 2D.

From the atomic-resolution image in Figure 2B, we identify the in-plane orientations of the graphene lattice within the two domains. We find that the smaller domain (colored red in Figure 2C) is rotated by ~17° with respect to the larger (green) domain. That is, for the smaller domain, the misorientation angle θ is ~23°. The atomic model

corresponding to θ = 23° is shown in Figure 2E. Note the absence of a moiré pattern. However, the STM image of the smaller domain in Figure 2A shows a stripe-like pattern. We suggest and justify below that this superstructure is part of the stripe patterns observed on the side facet (see Figure 2A).

Graphene on Ni(110). Figure 3A shows similar stripe patterns, with a spacing of ~12 Å, on the top surface of another Ni island. Figure 3B is an atomic-resolution STM image acquired from the region highlighted by a square in Figure 3A. From the Fourier transform of this image, we identify the spots corresponding to graphene 1 × 1 and Ni(110)-1 × 1 lattices and their relative orientations (see Figure 3C). Using these data, we constructed an atomic model of graphene/Ni (110) superstructure shown in Figure 3D, where the experimentally measured stripe pattern and periodicity are reproduced with θ = 25°. That is, the top surface facet orientation of the 3D Ni island in Figure 3 is (110).

We now return to the stripe patterns observed on the side facet of the Ni island in Figure 2. We suggest that these stripes are also due to superposition of graphene on Ni(110). From the STM image in Figure 2A, we determined the angle between the top (111) surface and the side facet to be ~38°. This value is closer to 35.3°, the angle expected between {111} and {110} facets. (We rule out {111} and {100} as possible orientations for the side facet because the expected angle between any two {111} facets is 70.5° and that between {111} and {100} facets is 54.7°.) The measured periodicity of the stripe pattern on the side facet is ~12 Å. In order to determine the orientation of graphene on the side facet, we calculated periodicities of stripe patterns as a function of θ. From the data plotted in Figure 4, in comparison with the STM measurements, we find that a periodicity of 12 Å is obtained when θ is 23.7°. Note that this value is approximately the same as the angle measured between Ni[110] and graphene [11$\bar{2}$0] on the top facet (red domain) in Figure 2C. This suggests that the graphene domains on the top (red) and the side facets have the same orientation; that is, the graphene domain grew seamlessly, as a single crystal, across adjacent (111) and (110) facets and over the facet boundary. Similar results have been reported for the growth of graphene on stepped Ni surfaces.[26,28] Moreover, calculations[26] suggest that the lowest energy configuration for graphene on Ni(110) is obtained when θ is ~24°. From these results, we suggest that the graphene domain (colored red in Figure 2C) formed on the (110) facet continued to grow over the adjacent (111) facet while maintaining the same crystalline orientation (*i.e.*, as a single crystal).

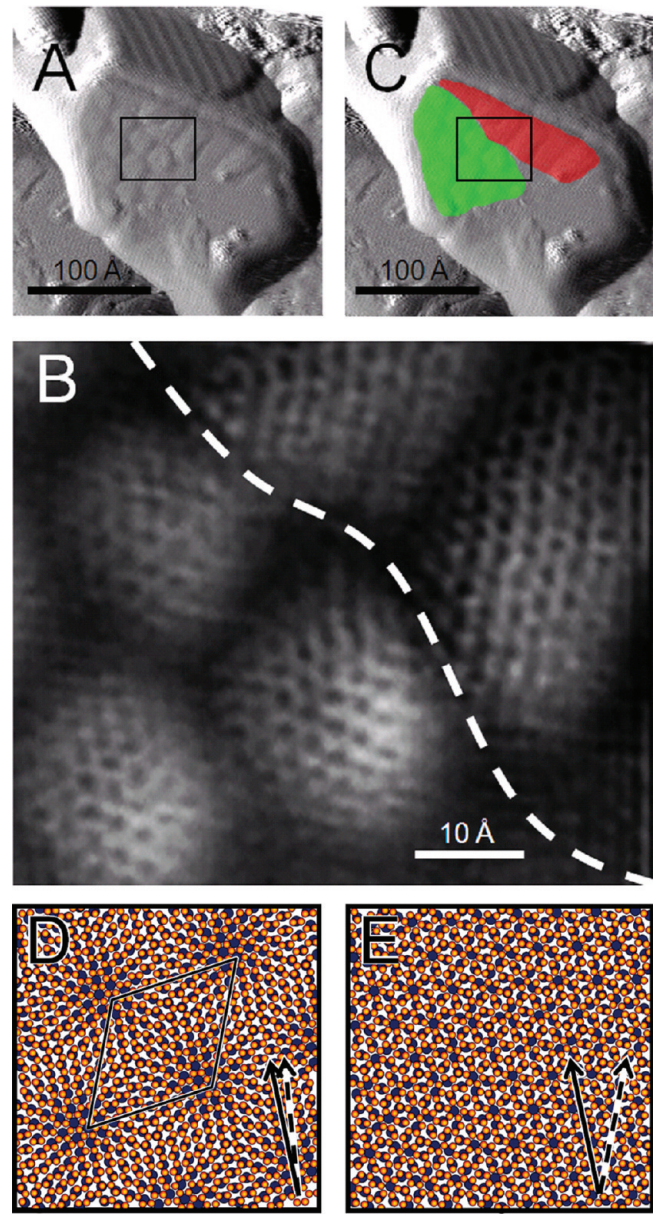

Figure 2. (A) STM image (250 × 220 Å^2) of a Ni(111) island. (B) Magnified image of the rectangular region highlighted in A. (C) Same as panel A, with the two graphene domains color-coded for clarity. Atomic models of Ni(111) (blue spheres) and graphene layer (orange spheres) rotated by (D) 6.4° and (E) 23° with respect to the Ni surface. The solid and dashed arrows indicate Ni[110] and graphene [11$\bar{2}$0] directions, respectively. The rhombus in D shows unit cell of a moiré pattern with a spatial periodicity of 22 Å.

Electronic Structure of Graphene on Ni(111) and Ni(110). We now focus on the electronic structure of graphene on Ni surfaces. We used point-mode STS and collected *I versus V* data from graphene on both Ni(111) and Ni(110). For comparison, we also collected STS data from pristine HOPG surface prior to Ni deposition and from the Ni islands prior to high-temperature annealing. The normalized conductance [(d*I*/d*V*)/(*I*/*V*)], extracted from the *I versus V* data, is expected to be nearly independent of the

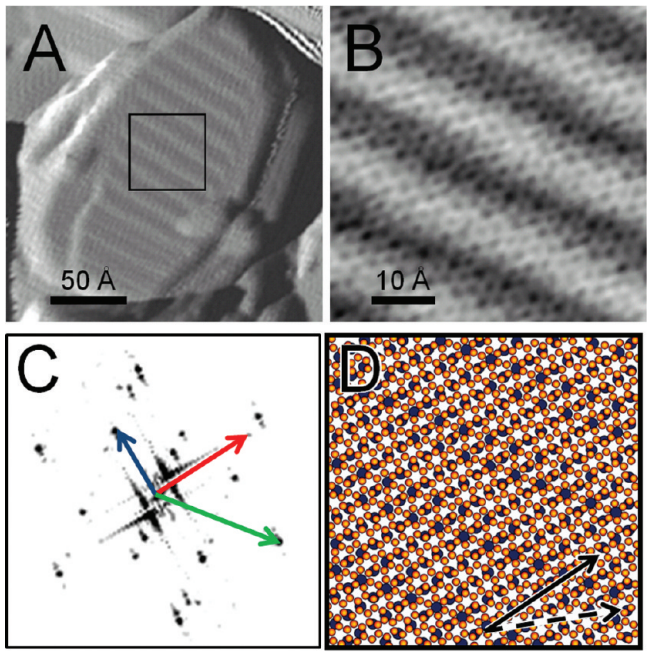

Figure 3. (A) STM image (207 × 207 Å^2) of a Ni(110) island. (B) Magnified image of the square area in A. (C) Fourier transform of panel B. Blue, red, and green arrows indicate Ni[100], Ni[110], and graphene [1$\bar{1}$00] spots, respectively. (D) Atomic model of Ni(110) (blue spheres) and graphene layer (orange spheres) rotated by 25° with respect to the Ni surface. The solid and dashed arrows show the Ni[110] and the graphene [11$\bar{2}$0] directions, respectively.

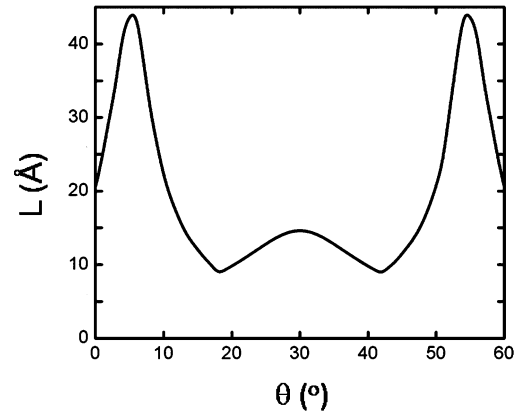

Figure 4. Stripe spacing L of the moiré patterns formed by graphene on Ni(110) as a function of the angle θ between the graphene [11$\bar{2}$0] and Ni [110].

tip−sample separation[29] and is a measure of the local surface density of states (LDOS). The [(dI/dV)/(I/V)] data plotted as a function of V in Figure 5A is an arithmetic average of values measured at over 100 different points on the surface. We find that the LDOS spectra for graphene on Ni(111) are qualitatively similar to that obtained from as-deposited Ni, and that the LDOS data for graphene on Ni(110) are similar to that of bare graphite surface. For both graphene/Ni(111) and graphene/Ni(110), we measure nonzero conductance values over a range of voltages centered around 0 V; that is, we do not observe an electronic band gap, indicative of metallic character. This result is typical of all of our STS measurements acquired using a range of tunneling currents from several different regions and Ni islands on the surface.

The observed metallic nature of the graphene layers on Ni surfaces is surprising. This is because the binding of graphene to both Ni(111) and Ni(110) is strong (~0.1 eV per carbon atom), in agreement with other DFT calculations[30] and recent experiments.[31] Furthermore, the carbon atoms in the two triangular sublattices of graphene have different relative locations with respect to the surface Ni atoms; that is, symmetry of the sublattices is broken and hence an opening of the band gap is expected[1,32] and was observed for graphene on Pd(111).[33] Indeed, our DFT calculations show that a band gap is opened for graphene on Ni at the K point, as seen in Figure 5B. However, the π*-band of carbon mixes strongly with the d-bands of Ni in other regions of the Brillouin zone. This hybridization of the Ni and C orbitals renders the graphene metallic, as the mixed bands cross the Fermi level between the Γ and the M points (see Figure 5B). To support these conclusions, we have calculated the density of states and have found that both the total (*i.e.*, with contributions from all atoms in the supercell and all angular momentum components) and the projected density of states (PDOS) corresponding only to the carbon atoms show no band gap (see Figure 5C). This result is consistent with the experimental LDOS data (Figure 5A). We note, however, that the agreement be-

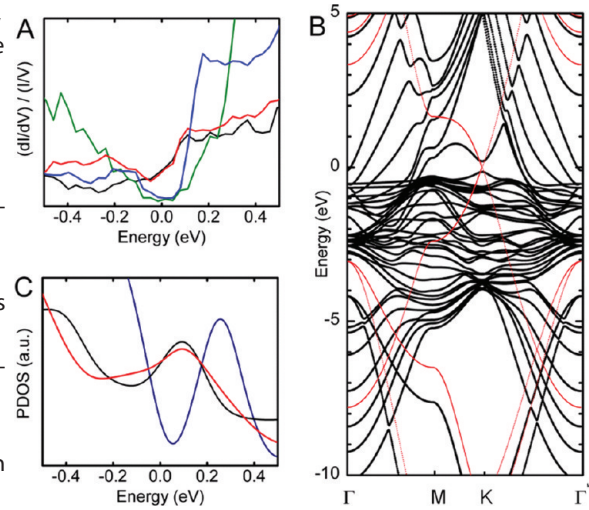

Figure 5. (A) STS spectra of graphene on a Ni(111) island (black), as-deposited Ni island (red), graphene on a Ni(110) island (blue), and clean HOPG surface (green). (B) Band structure of the graphene on Ni(111) system (black thick curves) as compared with the band structure of free-standing graphene (red thin lines). (C) Calculated projected density of states (PDOS) corresponding to carbon atoms and to all angular momentum and spin components for graphene on Ni(111) (black), pure Ni(111) surface (red), and graphene on Ni(110) (blue).

tween the DFT-calculated PDOS and the experimental LDOS results is only qualitative because of the small size of the unit cells used in the computations (see Methods section).

CONCLUSIONS

In conclusion, we used UHV-STM and investigated the growth and structure of graphene on (111) and (110) facets of 3D Ni islands. We observed hexagonal and striped moiré superstructures of graphene on (111) and (110) surfaces of Ni, respectively. We also find evidence for single-crystalline growth of graphene on adjacent facets of different orientation. STS measurements and DFT calculations for graphene layers on (111) and (110) surfaces of Ni yield local densities of states that do not vanish at the Fermi level, which is consistent with large binding energies (~0.1 eV per carbon atom) and strong hybridization between Ni and C bands. Our growth results suggest the possibility of single-crystalline growth over large areas with potential technological implications for low-cost, large-scale fabrication of graphene on polycrystalline metal thin films or foils. The metallic behavior of graphene on Ni surfaces is encouraging since the nature of the metal−graphene contact (Ohmic or Schottky) is important for graphene-based devices.

METHODS

Experimental: All of our graphene growth experiments were carried out on Ni films, ~3 Å thick, evaporated onto clean HOPG substrates using the procedure described below. First, 0.2 mm × 2 mm × 10 mm rectangular strips of HOPG were mechanically cleaved, placed on top of a polished SiC(0001) wafer (0.5 mm × 2 mm × 12 mm) coated with ~2000 Å thick Ta layer on the back side, and mounted together on to the Omicron VT-STM holder. The Ta thin film serves as the heater, and the SiC wafer helps prevent direct heating of the graphite. The holder was then transferred to a UHV multichamber (base pressure $<2 \times 10^{-10}$ Torr) STM system equipped with facilities for electron-beam evaporation and low-energy electron diffraction (LEED). The HOPG sample was degassed in UHV at 700 °C for 14 h. This procedure resulted in sharp 1 × 1 LEED corresponding to an in-plane atomic spacing of 2.46 Å. STM images showed atomically smooth terraces >1000 Å wide and separated by monolayer-height steps with a measured step height of 3.3 Å. Ni film was deposited at a rate of 0.002 monolayer/s *via* electron-beam evaporation in UHV at room temperature. The samples were then annealed at temperatures between 400 and 700 °C. Substrate temperatures were measured using optical pyrometry and are accurate to within 50 K. STM images were acquired in the constant current mode using commercially available Pt−Ir tips. Typical tunneling currents of 0.1 to 0.3 nA and bias voltages of −1.0 to +1.0 V were used. Pixel resolution in the images varied from 0.1 × 0.1 to 10 × 10 Å^2. Scan sizes (50−5000 Å), scan rates (50−100 s/frame), and tunneling parameters were varied to check for tip-induced effects. We observed no such effects in the results presented here. STM images were processed using WSXM software.[34] Point-mode STS measurements were obtained from the graphene layers at room temperature. In the STS mode, *I versus V* data were acquired over a range of bias voltages V_T between −1 and +1 V. During the measurements, tip−sample separation was held constant by interrupting the feedback loop.

Computational: DFT calculations were performed in the framework of the spin-polarized local density approximation, which was reported to perform well for graphene on Ni substrates.[35] We used ultrasoft pseudopotentials and the Ceperley-Alder exchange and correlation functionals, as implemented in the VASP package.[36,37] Structural relaxations were performed using monolayer graphene on six Ni(111) layers and five Ni(110) layers. Optimizations were carried out by allowing all the atoms to relax until residual forces were smaller than 0.01 eV/Å. Periodic boundary conditions were applied in the plane of the surface, and a vacuum thickness of 15 Å was introduced in the direction perpendicular to the surface. The structure of graphene on Ni(111) corresponds to a 1 × 1 reconstruction, where one carbon atom lies directly above a surface Ni atom and the other carbon atom lies atop the void site between three Ni atoms. The 1 × 1 slab is sufficient for providing an estimate of binding energy and qualitative insight into the electronic properties of graphene on Ni(111). This is because the misorientation between graphene and Ni(111) observed in STM experiments is relatively small (~6.4°). We used a cutoff for 400 eV for the energy of the plane waves. The Brillouin zone was sampled with a Monkhorst-Pack 8 × 8 × 1 for optimizations and 48 × 48 × 1 for calculations of the PDOS. For graphene on Ni(110), in-plane dimensions of the model supercell were 4.32 × 12.30 Å^2, and the *k*-point grids were 9 × 4 × 1 (relaxation) and 24 × 8 × 1 (PDOS analysis).

Acknowledgment. We gratefully acknowledge support from the University of California Discovery Grant, Northrop Grumman Space Corporation, and from the National Science Foundation through Grant Nos. CMMI-0825592 and CMMI-0846858. This work has benefited from the use of the facilities at the Frederick Seitz Materials Research Laboratory Center for Microanalysis of Materials and at the National Center for Supercomputing Applications at University of Illinois at Urbana−Champaign (Grant No. DMR-090121).

REFERENCES AND NOTES

1. Geim, A. K.; Novoselov, K. S. The Rise of Graphene. *Nat. Mater.* **2007**, *6*, 183–191.
2. Bunch, J. S.; Zande, A. M.; Verbridge, S. S.; Frank, I. W.; Tanenbaum, D. M.; Parpia, J. M.; Craighead, H. G.; McEuen, P. L. Electromechanical Resonators from Graphene Sheets. *Science* **2007**, *315*, 490–493.
3. Geim, A. K.; MacDonald, A. H. Graphene: Exploring Carbon Flatland. *Phys. Today* **2007**, *60*, 35–41.
4. Kim, K. S.; Zhao, Y.; Jang, H.; Lee, S. Y.; Kim, J. M.; Kim, K. S.; Ahn, J. H.; Kim, P.; Choi, J. Y.; Hong, B. H. Large-Scale Pattern Growth of Graphene Films for Stretchable Transparent Electrodes. *Nature* **2009**, *457*, 706–710.
5. Forbeaux, I.; Themlin, J. M.; Charrier, A.; Thibaudau, F.; Debever, J. M. Solid-State Graphitization Mechanisms of Silicon Carbide 6H-SiC Polar Faces. *Appl. Surf. Sci.* **2000**, *162*, 406–412.
6. Rosei, R.; De Crescenzi, M.; Sette, F.; Quaresima, C.; Savoia, A.; Perfetti, P. Structure of Graphitic Carbon on Ni(111): A Surface Extended-Energy-Loss Fine-Structure Study. *Phys. Rev. B* **1983**, *28*, 1161–1164.
7. Yu, Q.; Lian, J.; Siriponglert, S.; Li, H.; Chen, Y.; Pei, S. S. Graphene Segregated on Ni Surfaces and Transferred to Insulators. *Appl. Phys. Lett.* **2008**, *93*, 113103.
8. Kholin, N. A.; Rut'kov, E. V.; Tontegode, A. Y. The Nature of the Adsorption Bond between Graphite Islands and Iridium Surface. *Surf. Sci.* **1984**, *139*, 155–172.
9. Loginova, E.; Bartelt, N. C.; Feibelman, P. J.; McCarty, K. F. Factors Influencing Graphene Growth on Metal Surfaces. *New J. Phys.* **2009**, *11*, 063046.
10. Land, T. A.; Michely, T.; Behm, R. J.; Hemminger, J. C.;

Comsa, G. STM Investigation of Single Layer Graphite Structures Produced on Pt(111) by Hydrocarbon Decomposition. *Surf. Sci.* **1992**, *264*, 261–270.
11. Sutter, P. W.; Flege, J. I.; Sutter, E. A. Epitaxial Graphene on Ruthenium. *Nat. Mater.* **2008**, *7*, 406–411.
12. Oshima, C.; Nagashima, A. Ultra-Thin Epitaxial Films of Graphite and Hexagonal Boron Nitride on Solid Surfaces. *J. Phys.: Condens. Matter* **1997**, *9*, 1–20.
13. Li, X.; Cai, W.; An, J.; Kim, S.; Nah, J.; Yang, D.; Piner, R.; Velamakanni, A.; Jung, I.; Tutuc, E.; *et al.* Large-Area Synthesis of High Quality and Uniform Graphene Films on Copper Foils. *Science* **2009**, *324*, 1312–1314.
14. Li, X.; Cai, W.; Colombo, L.; Ruoff, R. S. Evolution of Graphene Growth on Ni and Cu by Carbon Isotope Labeling. *Nano Lett.* **2009**, *9*, 4268–4272.
15. Reina, A.; Jia, X. T.; Ho, J.; Nezich, D.; Son, H. B.; Bulovic, V.; Dresselhaus, M. S.; Kong, J. Large Area, Few-Layer Graphene Films on Arbitrary Substrates by Chemical Vapor Deposition. *Nano Lett.* **2009**, *9*, 30–35.
16. Shikin, A. M.; Farías, D.; Rieder, K. H. Phonon Stiffening Induced by Copper Intercalation in Monolayer Graphite on Ni(111). *Europhys. Lett.* **1998**, *44*, 44–49.
17. Nagashima, A.; Tejima, N.; Oshima, C. Electronic States of the Pristine and Alkali-Metal-Intercalated Monolayer Graphite/Ni(111) Systems. *Phys. Rev. B* **1994**, *50*, 17487–17495.
18. Gall, N. R.; Rut'kov, E. V.; Tontegode, A. Ya. Intercalation of Nickel Atoms under Two-Dimensional Graphene Film on (111)Ir. *Carbon* **2000**, *38*, 663–667.
19. Bäumer, M.; Libuda, J.; Freund, H. J. The Temperature Dependent Growth Mode of Nickel on the Basal Plane of Graphite. *Surf. Sci.* **1995**, *327*, 321–329.
20. Campos, L. C.; Manfrinato, V. R.; Sanchez-Yamagishi, J. D.; Kong, J.; Jarillo-Herrero, P. Anisotropic Etching and Nanoribbon Formation in Single-Layer Graphene. *Nano Lett.* **2009**, *9*, 2600–2604.
21. Ci, L.; Xu, Z.; Wang, L.; Gao, W.; Ding, F.; Kelly, K. F.; Yakobson, B. I.; Ajayan, P. M. Controlled Nanocutting of Graphene. *Nano Res.* **2008**, *1*, 116–122.
22. Datta, S. S.; Strachan, D. R.; Khamis, S. M.; Johnson, A. T. C. Crystallographic Etching of Few-Layer Graphene. *Nano Lett.* **2008**, *8*, 1912–1915.
23. Severin, N.; Kirstein, S.; Sokolov, I. M.; Rabe, J. P. Rapid Trench Channeling of Graphenes with Catalytic Silver Nanoparticles. *Nano Lett.* **2009**, *9*, 457–461.
24. Schäffel, F.; Warner, J. H.; Bachmatiuk, A.; Rellinghaus, B.; Büchner, B.; Schultz, L.; Rümmeli, M. H. Shedding Light on the Crystallographic Etching of Multi-Layer Graphene at the Atomic Scale. *Nano Res.* **2009**, *2*, 695–705.
25. Xu, M.; Fujita, D.; Sagisaka, K.; Watanabe, E.; Hanagata, N. Single-Layer Graphene Nearly 100% Covering an Entire Substrate. arXiv:1006.5085v1 [cond-mat.mtrl-sci].
26. Usachov, D.; Dobrotvoskii, A. M.; Varykhalov, A.; Rader, O.; Gudat, W.; Shikin, A. M.; Adamchuk, V. K. Experimental and Theoretical Study of the Morphology of Commensurate and Incommensurate Graphene Layers on Ni Single-Crystal Surfaces. *Phys. Rev. B* **2008**, *78*, 085403.
27. Loginova, E.; Nie, S.; Thürmer, K.; Bartelt, N. C.; McCarty, K. F. Defects of Graphene on Ir(111): Rotational Domains and Ridges. *Phys. Rev. B* **2009**, *80*, 085430.
28. Pan, Y.; Zhang, H.; Shi, D.; Sun, J.; Du, S.; Liu, F.; Gao, H. J. Highly Ordered, Millimeter-Scale, Continuous, Single-Crystalline Graphene Monolayer Formed on Ru(0001). *Adv. Mater.* **2009**, *21*, 2777–2780.
29. Feenstra, R. M. Scanning Tunneling Spectroscopy. *Surf. Sci.* **1994**, *299/300*, 965–979.
30. Khomyakov, P. A.; Giovannetti, G.; Rusu, P. C.; Brocks, G.; van den Brink, J.; Kelly, P. J. First-Principles Study of the Interaction and Charge Transfer between Graphene and Metals. *Phys. Rev. B* **2009**, *79*, 195425.
31. Grüneis, A.; Vyalikh, D. V. Tunable Hybridization between Electronic States of Graphene and a Metal Surface. *Phys. Rev. B* **2008**, *77*, 193401.
32. Han, M. Y.; Oezyilmaz, B.; Zhang, Y. B.; Kim, P. Energy Band-Gap Engineering of Graphene Nanoribbons. *Phys. Rev. Lett.* **2007**, *98*, 206805.
33. Kwon, S. Y.; Ciobanu, C. V.; Petrova, V.; Shenoy, V. B.; Bareno, J.; Gambin, V.; Petrov, I.; Kodambaka, S. Growth of Semiconducting Graphene on Palladium. *Nano Lett.* **2009**, *9*, 3985–3990.
34. Horcas, I.; Fernández, R.; Gómez-Rodriguez, J. M.; Colchero, J.; Gómez-Herrero, J.; Baro, A. M. WSXM: A Software for Scanning Probe Microscopy and a Tool for Nanotechnology. *Rev. Sci. Instrum.* **2007**, *78*, 013705.
35. Fuentes-Cabrera, M.; Baskes, M. I.; Melechko, A. V.; Simpson, M. Bridge Structure for the Graphene/Ni(111) System: A First Principles Study. *Phys. Rev. B* **2008**, *77*, 035405.
36. Kresse, G.; Furthmuller, J. Efficient Iterative Schemes for *Ab Initio* Total-Energy Calculations Using a Plane-Wave Basis Set. *Phys. Rev. B* **1996**, *54*, 11169–11186.
37. Kresse, G.; Furthmuller, J. Efficiency of *Ab-Initio* Total Energy Calculations for Metals and Semiconductors Using a Plane-Wave Basis Set. *Comput. Mater. Sci.* **1996**, *6*, 15–50.